infrastructures

MDPI

Article

Lateral Performance of Steel–Concrete Anchors Embedded in RC Columns Subjected to Fire Scenario

Amer Alkloub [1,*], Mahmoud Dwaikat [2], Ahmed Ashteyat [1,3], Farouq Sammour [1] and Asala Jaradat [1]

[1] Department of Civil Engineering, School of Engineering, University of Jordan, Amman 11942, Jordan; a.ashteyat@ju.edu.jo (A.A.); farouq@tamu.edu (F.S.); asajaradat@yahoo.com (A.J.)
[2] Department of Architectural and Civil Engineering, An-Najah National University, Nablus P4110257, Palestine; m.m.dwaikat@najah.edu
[3] Department of Civil Engineering, College of Engineering in Al-Kharj, Prince Sattam Bin Abdulaziz University, Al-Kharj 11942, Saudi Arabia
* Correspondence: a.kloub@ju.edu.jo

Abstract

The use of both structural steel and reinforced concrete is common in civil and military infrastructure projects. Anchorage plays a crucial role in these systems, serving as the key element that connects structural components and secures attachments within complex composite structures. This research focuses on evaluating the performance of steel–concrete column connections under the combined effects of lateral loading and fire exposure. Additionally, the study investigates the use of carbon fiber-reinforced polymers (CFRP) for strengthening and repairing these connections. The research methodology combines experimental testing and finite-element modeling to achieve its objectives. First, experimental investigation was carried out to test two groups of steel-reinforced concrete column specimens, each group made of three specimens. The first group specimens were designed based on special moment frame (SMF) detailing, and the other group specimens were designed based on intermediate moment frame (IMF) detailing. These two types of design were selected based on seismic demands, with SMFs offering high ductility and resilience for severe earthquakes and IMFs providing a cost-effective solution for moderate seismic zones, both benefiting from ongoing innovations in connection detailing and design approaches. Then, finite-element analysis was conducted to model the test specimens. High-fidelity finite-element modeling was conducted using ANSYS program, which included three-dimensional coupled thermal-stress analyses for the six tested specimens and incorporated nonlinear temperature-dependent materials characteristics of each component and the interfaces. Both the experimental and numerical results of this study show that fire has a more noticeable effect on displacement compared to the peak capacities of both types of specimens. Fire exposure results in a larger reduction in the initial residual lateral stiffness of the SMF specimens when compared to IMF specimens. While the effect of CFRP wraps on initial residual lateral stiffness was consistent for all specimens, it caused more improvement for the IMF specimen in terms of post-fire ductility when compared to SMF specimens. This exploratory study confirms the need for further research on the effect of fire on the concrete–steel anchorage zones.

Keywords: steel anchors; pedestal column; fire scenario; lateral performance; strengthening; reinforced concrete

Academic Editor: Darius Bačinskas

Received: 27 April 2025
Revised: 13 June 2025
Accepted: 23 June 2025
Published: 5 July 2025

Citation: Alkloub, A.; Dwaikat, M.; Ashteyat, A.; Sammour, F.; Jaradat, A. Lateral Performance of Steel–Concrete Anchors Embedded in RC Columns Subjected to Fire Scenario. *Infrastructures* **2025**, *10*, 173. https://doi.org/10.3390/infrastructures10070173

1. Introduction

In both civil and military construction, it is common to use structures that combine a steel superstructure with a reinforced concrete (RC) substructure, which often includes RC stub columns and footings. Steel is preferred for structural components in applications such as large factories, storage facilities, aviation hangars, and parking structures due to its construction advantages and suitability for specific design requirements (Figure 1). A typical example of this approach is found in the construction of storage facilities, where a steel superstructure is used to support relatively low gravity loads. In these cases, steel columns are anchored to reinforced concrete pedestals, which contain embedded anchorages. These anchorages are crucial for linking structural elements and securing attachments in modern composite or prefabricated constructions. The design provisions of these anchorages are available per international design codes.

Figure 1. Steel-reinforced concrete anchors in solar-mounted structure.

These anchorages are also found in structures that are susceptible to fire exposure, and their strength is crucial for ensuring the overall safety of the structure during and after fire exposure. The response of such systems to lateral loads before and after exposure to fire requires a thorough investigation.

The study includes reinforced concrete pedestals with two distinct reinforcement configurations: special moment frame (SMF) and intermediate moment frame (IMF). The lateral response of these configurations offers valuable insights into the performance and behavior of these crucial structural elements when subjected to fire exposure. The lateral response of CFRP (carbon fiber-reinforced polymer) wrapping to strengthen reinforced concrete pedestals under these configurations is also investigated after exposure to fire.

The selection of special moment frames (SMF) and intermediate moment frames (IMF) is primarily based on seismic design criteria, where SMFs are preferred in high-seismic zones due to their superior ductility, energy dissipation, and ability to sustain large inelastic deformations without collapse, while IMFs are more suited for moderate seismic regions, offering a compromise between performance and cost [1,2]. SMFs utilize advanced connection technologies—such as reduced beam sections (RBS) and welded flange-bolted web joints—that are specifically designed to allow plastic hinging in beams, improving overall structural resilience. IMFs, on the other hand, involve less rigorous detailing, making use of simpler connections that still provide moderate ductility, which is adequate for structures where seismic demands are lower [3]. Continued innovation in materials, connection detailing, and performance-based seismic design has enhanced the reliability and cost-effectiveness of both frame types in modern structural engineering.

CFRP wrapping presents an attractive and efficient solution for strengthening fire-damaged structural elements, largely due to its ease of application and rapid installation process. These characteristics are particularly valuable in scenarios where minimizing downtime is critical, such as in industrial facilities where operational interruptions can result in significant economic losses. The lightweight nature and high strength-to-weight ratio of CFRP materials further contribute to their suitability for retrofitting applications, enabling effective structural recovery without imposing substantial additional loads [4,5]. Moreover, CFRP systems can be installed with minimal surface preparation and without the need for heavy equipment, making them ideal for post-fire rehabilitation in constrained or sensitive environments [6].

While extensive research has been conducted on the performance of steel and concrete structural members—such as beams, columns, and slabs—under fire conditions, there has been limited focus on the behavior and strength of laterally loaded steel–concrete anchors when exposed to fire. This research gap has resulted in a lack of sufficient design guidance for these critical components. The primary objective of this study is to thoroughly investigate the post-fire lateral performance of steel–concrete anchors embedded in SMF and IMF reinforced concrete pedestals with or without strengthening CFRP wrapping. To achieve this, an experimental program was designed and executed, complemented by the development and use of finite-element modeling techniques.

2. Literature Review

An experimental study was investigated on the seismic behavior of a full-scale concentrically braced steel frame designed to Eurocode 8 (EC8) standards and equipped with various passive fire protection systems [7]. The study tested calcium silicate boards (standard and enhanced for seismic use) and mineral spray-based fire protections applied to both dissipative and non-dissipative structural elements. Two types of concrete block fire walls—one with and one without seismic detailing—were also included. Ten tests were conducted on four frame configurations under different seismic intensities using a hybrid simulation technique, where only the ground floor was physically tested, while the upper structure was numerically modeled. Results showed that neither the fire protections nor the fire walls experienced significant damage under cyclic loading, indicating their fire performance would remain largely unaffected by seismic events.

The flexural performance was investigated of an integrated laced steel–concrete composite (i-LSCC) panel, formed by connecting three LSCC units with bolted flanges for efficient load transfer [8]. Experimental and numerical analyses were conducted to evaluate its behavior under different loading directions. Static tests showed that the units acted as a cohesive panel, with similar peak loads and displacements regardless of loading direction. Failure occurred due to tearing of the bottom cover plates, with support rotations aligning closely with design targets. Finite-element analysis (FEA) closely matched experimental results in the linear range, slightly overestimating load and underestimating displacement, while accurately capturing failure modes. The findings confirm the i-LSCC panel's strong ductile performance and suitability for blast-resistant structures, offering both resilience and construction efficiency.

The limited research was addressed on the fire performance of high-strength materials in composite columns, examining concrete-encased steel (CES) columns under fire conditions through experiments and simulations [9]. Five CES specimens were tested under varying load eccentricities. Polypropylene fibers were added to prevent explosive spalling, eliminating the need to model this effect numerically. A unified method was developed to define the transient strain of high-strength concrete at elevated temperatures, extending existing stress–strain models to C120. A new numerical model was introduced to predict

axial displacement by accounting for strain reversal due to flexural deformation. Using this model, a new tabulated method for fire resistance design was proposed for CES columns with concrete grades up to C90 and steel grades up to S550.

The post-fire performance was investigated of steel reinforced concrete (SRC) columns, highlighting that concrete encasement helps limit steel temperature during fires [10]. Key factors influencing residual strength include fire duration, cross-section size, slenderness ratio, and concrete strength. The compressive resistance of the SRC column decreased by 4% following fire exposure. However, with the proposed repair method, it can be enhanced by 11% relative to its pre-fire condition. A variety of single-headed stud anchors that were subjected to varied lengths of time under fire was investigated and were loaded in shear perpendicular to and towards the free concrete edge until failure after cooling [11]. At varied fire durations, the influences of concrete edge distance, nominal diameter, embedment depth, and concrete compressive strength on the load-bearing behavior of the anchors were explored empirically. The effect of fire on the residual capabilities of the anchors was studied using the ISO-834 standard fire curves with corresponding durations of 15 and 60 min [12]. The findings showed that fire exposure has a major impact on anchor behavior. Under ambient circumstances, the edge distance has a significant impact on anchor resistance, whereas the anchor diameter and embedment depth have a minor impact. The impact of the edge distance on shear resistance decreases following fire contact, whereas the influence of the diameter and embedment depth on shear resistance improves. The impact of fire exposure on the concrete edge strength of anchors is substantial. The loss of more than 50% of the reference value was recorded after only 15 min of fire intensity.

Spalling is a significant reaction on fire-exposed concrete that can destroy whole cross-sections or significantly reduce a structure's load-bearing capability. When developing a fire-resistant concrete structure, spalling must be considered. Hertz [13] established parameters within which spalling should not occur as well as some suggestions for lowering the danger of spalling for structures that exceed the safe design limitations, based on study and practice. Hertz's findings show that conventional concretes within 3 wt.% moisture do not require documentation for spalling resistance; however, it is advised that this remark be included in the structural regulations [13]. In addition, the spalling resistance of dense concrete must be demonstrated using a full-scale test with the appropriate humidity, stresses, and boundary conditions. It is also advised that constructions be designed with loadbearing areas of the cross-section that are as porous and dry as possible to avoid the possibility of spalling. According to the findings, polypropylene fibers could avoid spalling of chosen slabs and unloaded specimens but not compressed structures or drilled tunnels.

Little evidence has been established for the fire performance of steel and concrete composite floor structural systems exposed to ISO fire conditions, and this lack of evidence continues to be a barrier for some national authorities to fully accept the design concept derived from Cardington real fire tests, particularly for long-duration ISO fires.

3. Experimental Program

A total of six specimens were constructed, each comprising a reinforced concrete (RC) footing and column, with an attached structural steel column. The experimental program involved categorizing these specimens into two distinct groups, based on the transverse reinforcement details of the RC columns in each specimen. The first group encompassed reinforced concrete columns that were designed and detailed to meet the specifications for special moment frames (SMF), as outlined in the ACI 318-25 code [14]. The second group was designed and detailed to simulate columns within intermediate moment frames (IMF).

3.1. Details of Specimens

Each group of this experimental program was composed of three identical specimens, with two of them subjected to the same fire scenario, as described later, while the third specimen was tested at room temperature. Notably, one of the specimens exposed to the fire scenario was retrofitted with carbon fiber-reinforced polymer (CFRP) sheets prior to the application of the lateral load. During the testing phase, a lateral load was applied to the free end of the steel section for each specimen.

All of the specimens were comprised of reinforced concrete (RC) footings and RC columns supporting structural steel columns, which exhibited identical dimensions and geometry across all specimens. The specimens' details are presented in Table 1 and shown in Figure 2. The RC columns were designed as SMF or IMF based on ANSI/AISC 360-22 [15], and the reinforcement details are presented in Figure 3a,b. Across all groups, the footings and structural steel columns were consistently detailed.

Table 1. Details of specimens that were constructed and tested in this research.

Group	Specimen	Use of CFRP	Fire Exposure	RC Columns			
				Cross-Section (mm × mm)	**Long. Reinf. (mm)**	**Trans. Reinf. (mm)**	**Crossties (mm)**
1	IMF-FE *	no	Exposed	300 × 300	(8)ϕ16 mm	ϕ10 mm @125 mm	-
	IMF-FE *-R	yes	Exposed	300 × 300	(8)ϕ16 mm	ϕ10 mm @125 mm	-
	IMF-NFE **	no	Room temp.	300 × 300	(8)ϕ16 mm	ϕ10 mm @125 mm	-
2	SMF-FE *	no	Exposed	300 × 300	(8)ϕ16 mm	ϕ10 mm @75 mm	ϕ10 mm
	SMF-FE *-R	yes	Exposed	300 × 300	(8)ϕ16 mm	ϕ10 mm @75 mm	ϕ10 mm
	SMF-NFE **	no	Room temp.	300 × 300	(8)ϕ16 mm	ϕ10 mm @75 mm	ϕ10 mm

* FE: fire exposure; ** NFE: no fire exposure.

The steel section has a depth of 260 mm, with top and bottom flanges measuring 200 mm in width and 12 mm in thickness. The web thickness is 12 mm. The steel section was affixed to the RC column by using 15 mm thick steel base plate, with the steel base plate measuring 200 square millimeters and the steel plate measuring 260 mm by 260 mm. Four ϕ20 mm anchor bolts were placed at the corners, with edge distances to the center of the bolt measuring 55 mm on the direction of loading and 65 mm on the other side. All the bolts are 20 mm in diameter with embedment depth of 160 mm. The distance between the anchor bolts is 150 mm center-to-center in both directions. Figure 3c shows the dimensions and detailing anchorage, which are typical in all specimens. The sequence of the construction of specimens is shown in Figure 4.

The RC footing has a rectangular shape, with dimensions of 580 mm (width) by 1450 mm (length, in direction of loading) and 250 mm in thickness. The footing is reinforced with top and bottom longitudinal reinforcement of eight bars ϕ16 mm and transversely reinforced with ϕ16 hoops spaced at 125 mm on center. The RC column was centered within the footing for all specimens, with their embedded reinforcement extending into the footing and forming a 90-degree hook.

The average mechanical properties for structural steel, steel stud, and steel reinforcement bars were measured by standard coupon tests. These results are presented in Table 2.

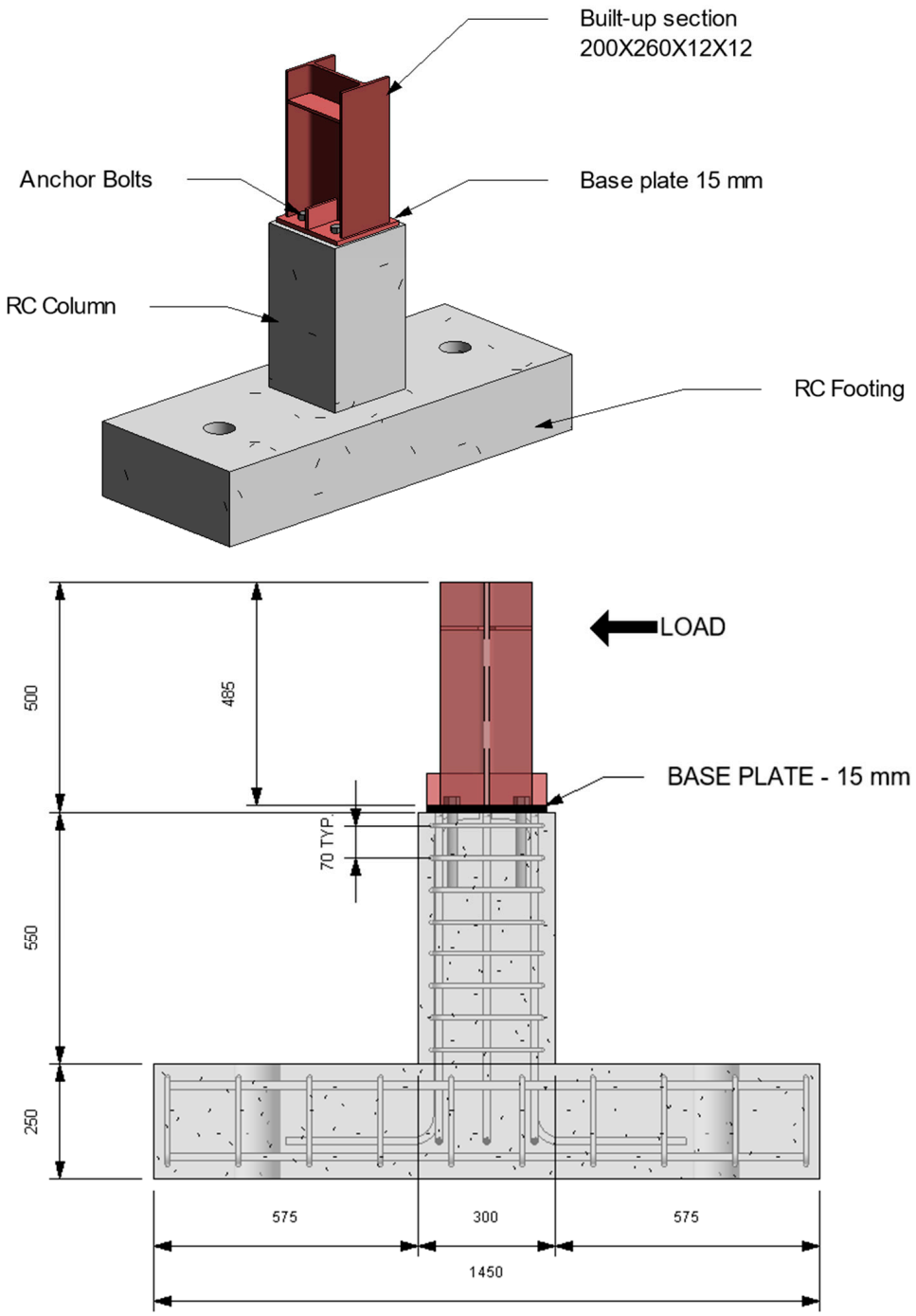

Figure 2. Details of geometry and anchorage of constructed specimens.

Table 2. Material properties of steel members (provided by manufacturer).

Member	Yield Strength f_y [MPa]	Ultimate Strength f_u [MPa]	Modulus of Elasticity E_s [GPa]
Steel section	355	450	200
Rebar	420	620	200
Stud	534	550	200

The CFRP sheet used for strengthening specimens had the material properties presented in Table 3. The CFRP was installed by painting the surface of concrete with a layer of epoxy using a plastic roller to bond the CFRP sheet, then wrapping one layer of CFRP sheet onto the column by passing roll-on. After that, the second layer of layer of epoxy was applied above the first CFRP sheet, and finally, another layer of CFRP sheet was wrapped onto the first layer of CFRP sheet by passing roll-on column. Table 4 presents the properties of the epoxy.

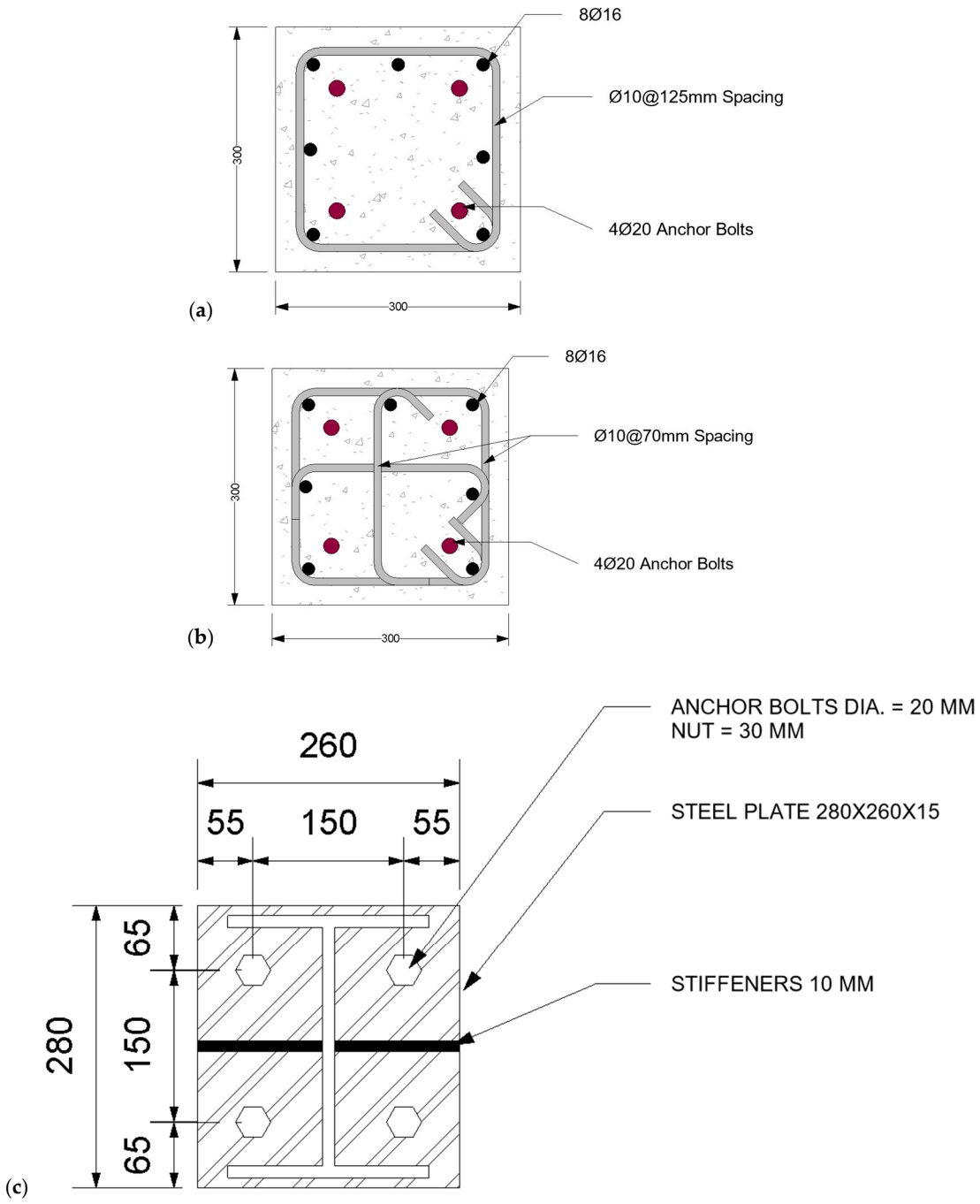

Figure 3. Details of (**a**) reinforcement based on IMF specifications, (**b**) reinforcement based on SMF specifications, and (**c**) anchorage of all specimens.

Figure 4. Photos of construction procedure of specimens.

Table 3. Properties of CFRP materials.

Property	Value
Modules of elasticity (GPa)	230
Tensile strength (MPa)	4900
Fiber density (g/cm^3)	1.8
Cross-section (mm^2)	167/m width
Elongation at break	1.7%

Table 4. Properties of Epoxy.

Property	Value
Packaging	5 kg A + B (light grey)
Density (kg/L)	1.3 ± 0.1
Tensile strength (MPa)	30
Elastic modules (MPa)	4500
Mixing ratio	A:B = 4:1 part by weight
Elongation at break	0.9%

3.2. Fire Exposure

An oven with external dimensions of 2 m × 1.5 m × 0.6 m, as shown in Figure 5, was used to expose the structure to a high temperature of 600 °C. The temperature and heating time were controlled by an electronic panel beside the electric furnace. After reaching 600 °C, the temperature was kept constant for three hours. The temperature history implemented in this study is displayed in Figure 6.

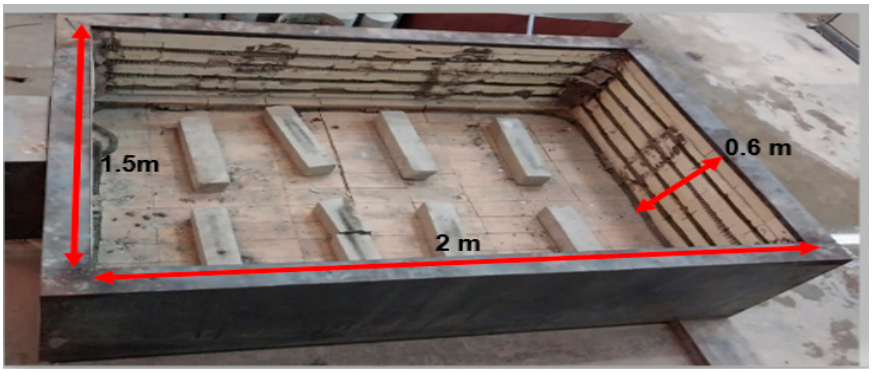

Figure 5. The oven used to apply high temperature.

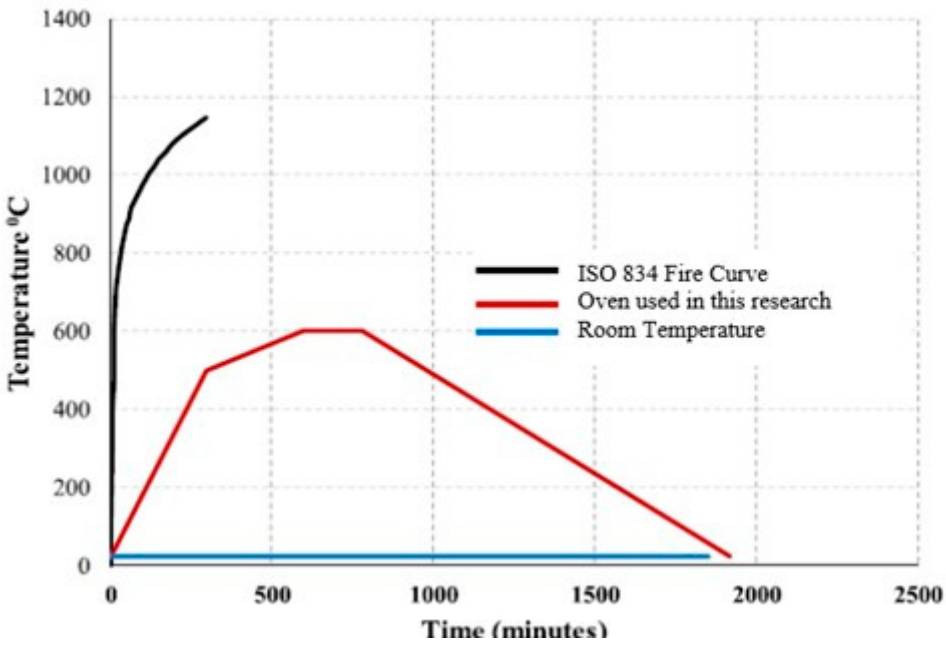

Figure 6. Time–temperature curves of heat-exposed specimens.

3.3. Test Setup

All specimens were subjected to static monotonic lateral load until failure (Figure 7). For specimens strengthened with CFRP, the installation of the CFRP sheets was carried out after the cooling phase of the fire exposure. Then, the specimen was loaded to failure. The breakout failure mode of the four bolts anchor group was investigated. The anchors were loaded perpendicular to and towards the free edge before and after fire exposure.

Figure 7. Test setup of all specimens in the experimental program.

4. Experimental Results

4.1. Mechanical Properties

The compressive strength of 300 mm concrete cubes and splitting tensile strength of 150 mm diameter and 300 mm height concrete cylinders used to cast footings and columns are presented in Tables 5 and 6, respectively.

Table 5. Results of cube compressive strength.

Concrete in	Fire Exposure	Test Days After Cast	Cube Strength (MPa)	Equivalent *f'c* (MPa)
Columns	no	28	48.1	38.5
	no	107	56.1	44.9
	yes	107	59.7	47.8
Footings	no	14	50.1	40.1
	no	130	59.7	47.8

Table 6. Results of splitting tensile strength.

Concrete in	Fire Exposure	Test Days After Cast	Splitting Strength (MPa)
Columns	no	28	12.2
	no	49	15.6
	yes	49	5.6
Footings	no	118	10.4
	no	130	10.4

4.2. Lateral Response

The response of specimens to lateral loads was investigated. The lateral load capacity strength and the corresponding lateral displacement are presented in Table 7 for specimens in group 1 and Table 8 for specimens in group 2. The load–displacement relationships of tested specimens are presented in Figure 8.

Table 7. Results of lateral response of specimens in group 1.

Specimen	Fire Exposure	RC Column (mm × mm)	Ultimate Force (kN)	Lateral Disp. (mm)
IMF-FE	Exposed		87	11.8
IMF-FE-R	Exposed		104.3	20.3
IMF-NFE	Room temp.		70.8	7.7

Table 8. Results of lateral response of specimens in group 2.

Specimen	Fire Exposure	RC Column (mm × mm)	Ultimate Force (kN)	Lateral Disp. (mm)
SMF-FE	Exposed		100.4	15.2
SMF-FE-R	Exposed		129.9	20.6
SMF-NFE	Room temp.		99.4	12.3

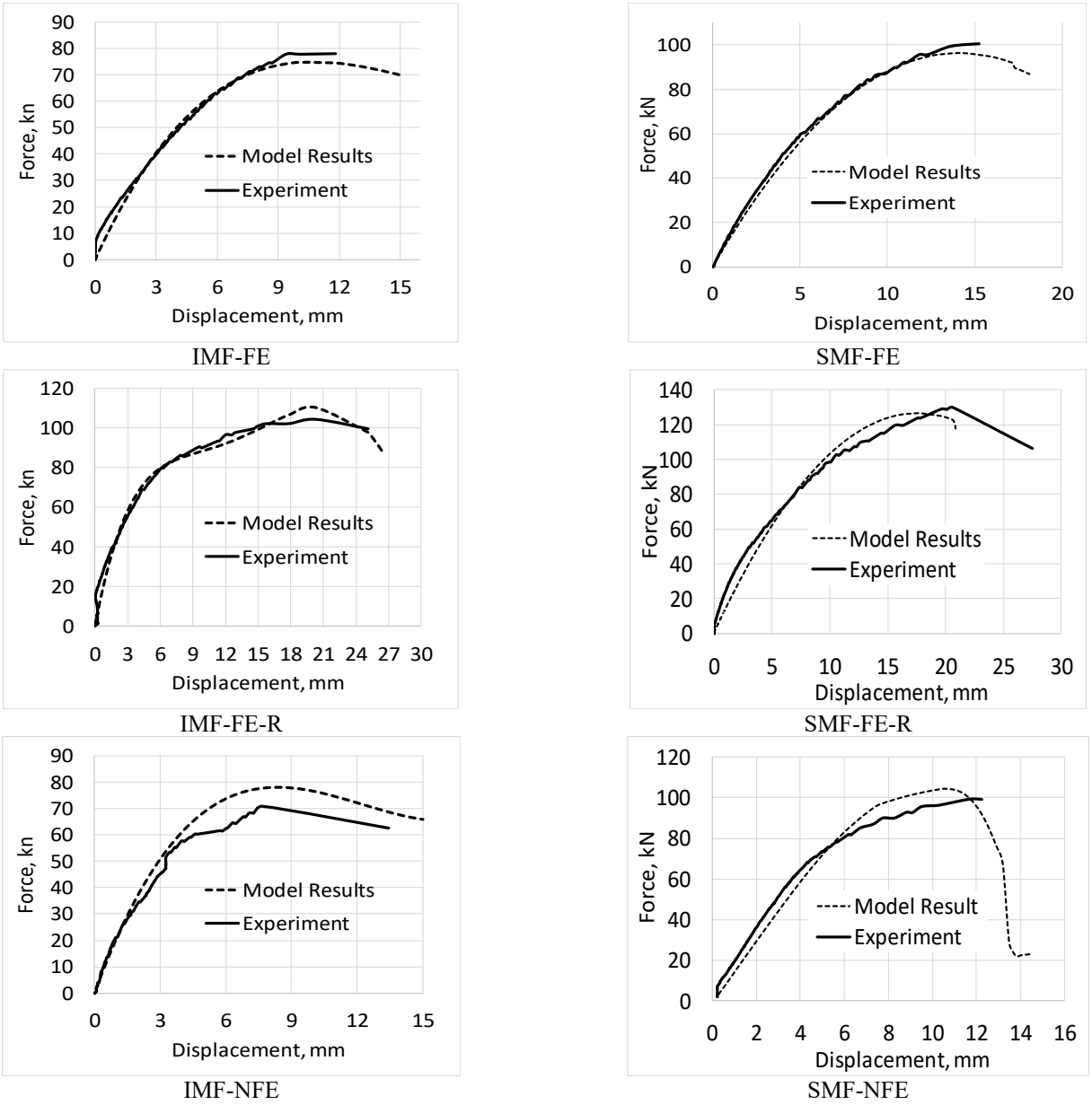

Figure 8. Comparing predictions from the FE model against the experimental results.

The observed mode of failure for all specimens was characterized by concrete breakout occurring on the tension side.

Generally, the fire exposure resulted in a more pronounced effect on the initial lateral residual stiffness but in a relatively smaller effect on the peak capacities of the specimens. For example, by comparing the SMF specimens without CFRP at a displacement of 1 mm, a reduction in strength (and thus in initial lateral stiffness) from 20 kN to 14 kN (30%) was measured due to fire exposure. The same comparison at the same displacement for the IMF specimens showed a smaller corresponding reduction in the initial stiffness: nearly 20%, from 18 kN to 15 kN. The change, however, in peak residual capacities is not significant due to fire for both specimens.

It can also be seen that fire exposure also resulted in larger failure displacements for all specimens, which is not unexpected. It can be understood that the differential thermal expansion could have caused interior slippage of anchorage, which degraded the overall lateral stiffness, as mentioned in the previous paragraph, thus leading to larger failure displacements. The increase in failure displacement due to fire is nearly 25% for both types of specimens.

An interesting overall result shows that there seems to be a slight gain in strength due to fire exposure. This is, in fact, not uncommon. Generally, some types of concretes experience an increase in residual strength when exposed to fire below 500 °C. Because of the high thermal insulative properties of concrete, the temperature inside the column stubs was mostly below 500 °C, as indicated by the results of the thermal analysis later on in this study. However, due to the differential thermal expansion, the interface of the anchors between steel and concrete could have suffered some degradation, which explains the higher lateral deformations in the specimens, as reported in the table. Also, the use of CFRP after fire exposure significantly improved the lateral strength but also led to an increase in lateral displacements.

Further, as seen in Figure 8, the CRFP wrapping significantly improved both the ductility and lateral residual strength of the specimens. An interesting observation is that the CFRP wrapping had almost a consistent effect on the residual initial lateral secant stiffness for both the SMF and IMF specimens. For the SMF specimen after fire exposure, the lateral strength at 1 mm displacement increased from 14 kN without CFRP to 22 kN after using CFRP, which is a 57% improvement. Likewise, the same comparison for the IMF specimen shows that the CFRP wraps had a similar effect on residual lateral stiffness, and at 1 mm displacement, the use of CFRP increased the lateral strength from 15 kN to 24 kN (60% improvement).

However, the use of CFRP seems to cause larger diversity in the post-fire ductility of both types of specimens. By comparing the displacements that correspond to the peak values of the lateral resistances of all specimens, we can see that the SMF had a 33% increase in post-fire ductility, while for IMF, it was 100%.

5. Finite-Element Modeling

The experiments were modeled using ANSYS software 2023 [16]. High-fidelity three-dimensional finite-element models were constructed using many types of elements and incorporating mechanical and the thermal temperature-dependent nonlinear properties of the materials. Figure 9 shows the general mesh details of the FE model for one of the tests. The structural steel, anchor rods, and the concrete were modeled using coupled-field SOLID226 elements with 20 nodes per element. SOLID226 element allows the capture and interaction of both stress and temperature fields within the solids due to its thermal–structural coupling. The steel reinforcements were explicitly embedded inside the concrete elements using finite-strain 1D LINK180 axial elements that are perfectly bonded to concrete. The interfaces between concrete and the structural steel section as well as between steel plates and the head of the anchor bolts were modeled as frictional interfaces with Columb coefficient of static friction = 0.3, which was adopted from Xu et al. [17]. The CFRP wraps were modeled using the 8-noded SHELL281 elements. The bond between the concrete and the CFRP was assumed to be perfect. However, the interface between anchor rods and concrete was assumed to be cohesive and was thus modeled using cohesive zone elements and materials, as explained later.

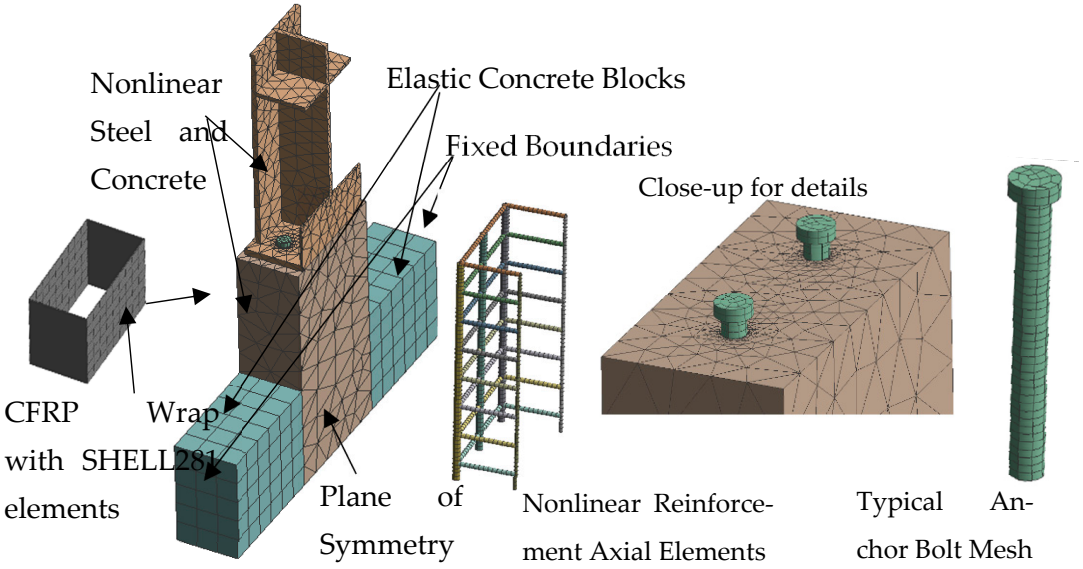

Figure 9. Mesh details for the finite-element half-model.

The input temperature-dependent mechanical material properties that were used in the simulations are shown in Figures 10 and 11 and were adopted from Kodur et al. [18]. The normalized stress–strain curves for both concrete and the reduction factors for steel and concrete are shown in Figure 10. The steel is assumed to follow a perfectly elastic–plastic stress–strain curve with temperature reduction factors for both yielding and elastic moduli, as shown in Figure 10a. The concrete is assumed to follow nonlinear stress–strain curves, as shown in Figure 10b, with the temperature degradation ratio of its compressive and tensile strengths shown in Figure 10a. For the thermal analysis, the temperature-dependent variation of the thermal strain for both steel and concrete is considered and shown in Figure 11. The thermal strain is an important factor in the coupled thermal–mechanical analysis because it produces the heat-induced thermal strain and stresses inside the specimens due to heating and cooling. Thermal analysis is presented in the subsequent section.

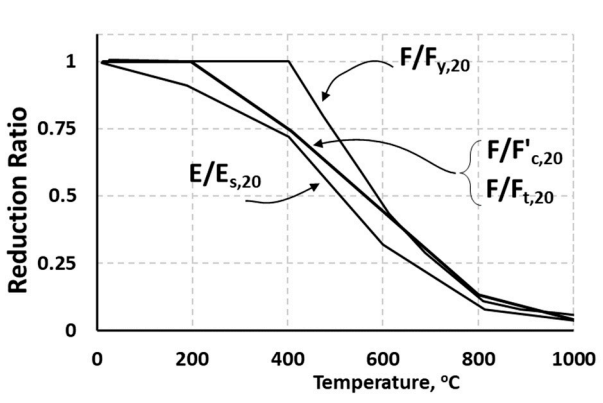

(**a**) Temperature-dependent reduction factors.

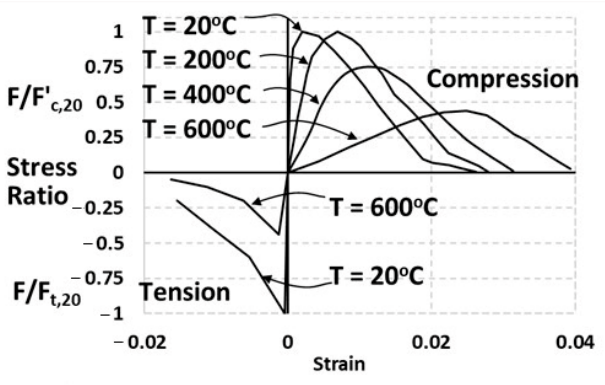

(**b**) Concrete temperature-dependent stress–strain.

Figure 10. Mechanical properties as a function of temperature, (**a**) strength and stiffness reduction factors for steel and concrete, and (**b**) the normalized temperature-dependent stress–strain curves for normal concrete.

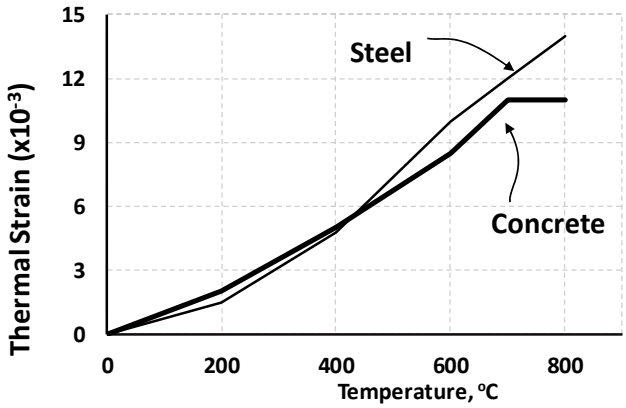

Figure 11. Thermal strain for all types of steel and for concrete.

The mechanical behavior of the materials during the cooling phase was assumed to trace back through the same path taken during the heating phase. This assumption is realistic for steel when exposed to temperature below 500 °C, but it is conservative for some types of concretes at temperature below 500 °C.

Cohesive zone elements were used to model the interface between the anchor rods and the concrete. Contact and target elements (CONTA174 and TARGE170) were generated at the interface between shear connectors and concrete, and the cohesive zone material (CZM) model was adopted to capture the adhesion stresses that occur between concrete and shear connectors. Figure 12 shows the material constitutive definition for the CZM under pure normal and shear stresses. These bi-linear relationships for defining the CZM are based on the model suggested by Alfano and Crisfield [19] and Alfano [20], which allows for a softening (or damage) effect in the cohesive zone material behavior upon reloading.

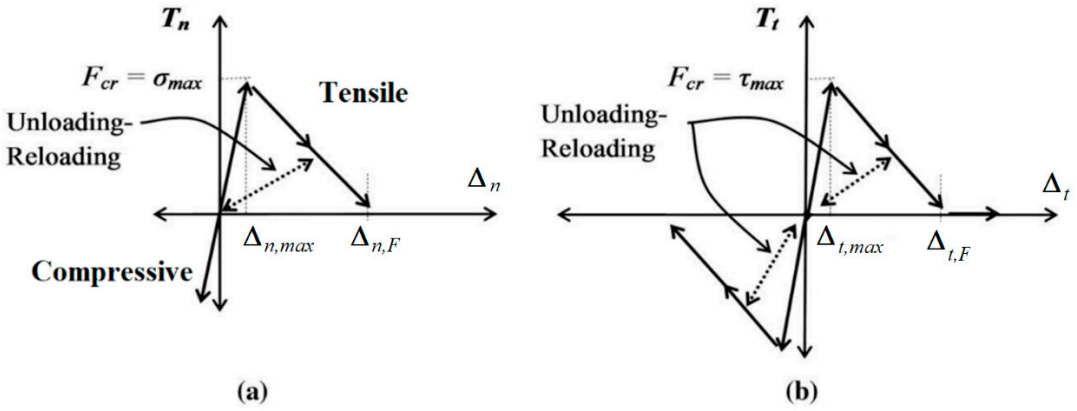

Figure 12. Material laws for cohesive zone material model under (**a**) pure normal and (**b**) pure shear stresses.

The failure in the CZM under mixed-mode debonding was established based on an interaction relationship between ratios of fracture energies due to both normal and shear tractions using the following equation:

$$\frac{G_n}{G_{n,cr}} + \frac{G_t}{G_{t,cr}} = 1.0$$

where G_n and G_t are the fracture energies due to pure normal and pure shear tractions, respectively. The $G_{n,cr}$ and $G_{t,cr}$ are the critical fracture energies that cause complete

debonding in either normal or shear mode, respectively. The fracture energy up to a slip "x" is defined as

$$G_x = \int T_x d\Delta_x$$

where T_x is the traction for either normal mode or shear mode, and Δx is the separation vector from either mode.

It is difficult to quantify the parameters needed for the CZM model for the embedded shear stud. The source of the difficulty is that most experiments are, in fact, pull-out tests of steel studs, which generally result in mostly shear dominated failure modes or concrete rupture under fully symmetric conditions. To the authors' knowledge, there is hardly any experiment that quantifies debonding of the concrete–steel interface under pure normal traction. Also, the majority of the experiments report overall pull-out displacements and not slip at debonding states.

In our model, the input parameters for the CZM are obtained from the literature based on bond-slip experiments of [21–25]. For example, ref. [26], in their ABAQUS modeling of their experiments on groups of shear studs, assumed a frictional cohesive model where the peak contact shear stress is taken to increase linearly up to 0.9 MPa at a slip of 0.06 mm; thereafter, the interfacial frictional stress remains constant. In their tests, the concrete had a compressive strength of 47 MPa and the studs a tensile strength of 530 MPa. On the other hand, Nguyen and Kim [27] used a bi-linear form of the CZM, where the initial stiffnesses were assumed to be 10% of the Young and shear moduli for both normal and shear traction components, respectively. However, in their ABAQUS model, the CZM model was based on strains rather than on slippage, and they defined the critical strains for normal and shear tractions to be 0.0001 and 0.0005, respectively, and the complete debonding state to occur at a failure slip of 0.8 mm. The justification for such numbers is that they produced the best results to fit the experiments performed by Lee et al. [28].

Based on the size of the cohesive elements used by Nguyen and Kim, the critical strains used corresponded to critical slips of 0.1 mm and 0.5 mm for normal and shear tractions, respectively, for concrete of compressive strength of 50 MPa. Lin et al. [29] used multi-linear relationships for the CZM and assumed a peak shear stress and slip of 0.41 MPa and 0.1 mm and the peak normal stress and slip of 0.1 MPa and 0.003 mm, respectively, for concrete compressive strength of 56 MPa.

While the literature is full of input values for the CZM modeling of the concrete–stud interface at room temperature, there is a lack of information about such parameters during and after high-temperature exposure. In the studies [30,31], the composite concrete–steel slabs with shear studs were tested and modeled under high temperature, and the CZM behavior was assumed to follow a coulomb-type friction model with a coefficient of 0.47. In other words, pure tensile resistance was neglected, and this led to a good match to the experimental results reported in these studies.

Thermal Analysis

The heat transfer analysis was modeled using SOLID226 coupled-field element. Because the furnace is electric and has no fans inside, the heat transfer was modeled through radiation only. The radiosity method is implemented to capture the radiation effect from the electric heater to specimen surface. And the enclosure was defined to be bounded by the walls of the furnace and the surfaces of the specimen. This allows for automatic computation of the view factor, and thus, the shielding effect was also modeled in this method. The temperature of the enclosure was taken to be equal to the furnace-recorded temperature curve. Different values of effective emissivity factor (e_e) were used depending on the exposure boundary and material [32]. The value of e_e = 0.7 for the outer-side surfaces of the concrete blocks and the web of the steel section and the value of e_e = 0.5 for

the internal sides of the steel flanges and the concrete inner faces were used. The Stefan–Boltzmann radiation constant of $\sigma = 5.679 \times 10^{-8}$ W/(m^2 K4) was used in the analysis. The temperature-dependent thermal properties of steel and concrete were taken from the literature. The interfaces were assumed thermally perfectly bonded. The radiosity analysis was solved using the Gauss–Seidel iterative solver with a tolerance of 0.001, as defaulted in ANSYS software. Figure 13 shows a cross-sectional view of the temperature distribution inside the specimen at 3 h into heat exposure. The analysis shows the lag in temperature distribution within the specimen, with the temperature in the steel section being on average hotter than that inside the concrete due to the shielding effect of the concrete blocks, which affects radiation heat transmission inside the furnace. The variation in the temperature field is obvious in the figure, which leads to variation in thermal strains.

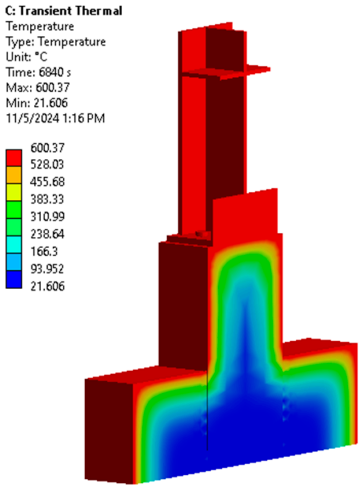

Figure 13. Cross-sectional temperature distribution (°C) from the thermal analysis after 3 h in the furnace.

In Figure 14, a comparison is made between the prediction from the finite-element model and the experimental observation. In this figure, von-Mises stresses were plotted. An acceptable match can be seen when compared to the observed failure pattern in the experiment such that that the tension failure facilitated the pull out of the anchored rods.

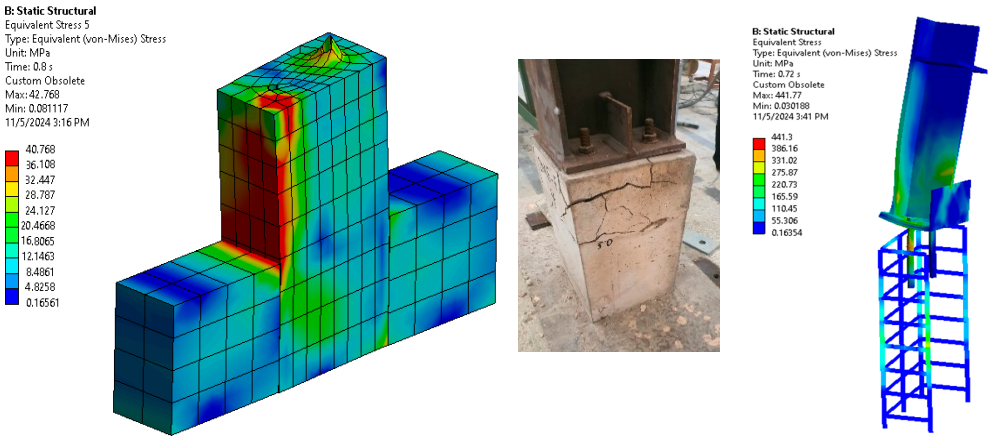

(**a**) VM stress in concrete. (**b**) Observed failure. (**c**) Stress in steel.

Figure 14. Comparing results for the specimen IMF-FE and (**a**) von-Mises equivalent stresses at time of failure, where the crushing is shown to happen near the compressed region; (**b**) the observed failure pattern; and (**c**) stresses in the steel, anchor bolts, and reinforcement. While the anchor rods and structural steel reached the yielding point, the reinforcement remained elastic.

The summary of the numerical results for the load–displacement relationships of tested specimens are presented in Figure 8. It can be concluded that the numerical results capture the experimental outcomes well and could trace the response up to and beyond failure.

6. Conclusions

This research examined the performance of steel–concrete column connections under lateral loading and fire exposure. It also explored the use of carbon fiber-reinforced polymers (CFRP) for strengthening and repairing these connections.

The experimental and numerical results showed that fire had a noticeable effect on the stiffness and displacement of the specimens, while it had a lesser effect on the residual capacity. The effect on stiffness was larger for the SMF specimens when compared to IMF. This could be due to the combination of both the confinement effect and differential thermal expansion in the specimens. The SMF specimen has a higher confinement effect due to the special stirrups detailing, and when combined with differential thermal expansion, the internal damage is expected to be larger, thus leading to a noticeable effect on initial residual stiffness.

The conclusions can be stated as follows.

1. Failure Mode

All tested specimens exhibited a consistent failure mode characterized by concrete breakout on the tension side, indicating tensile failure in the concrete due to insufficient resistance to applied lateral forces.

2. Effect of Fire Exposure

Fire exposure had a significant degrading effect on the initial lateral stiffness of the specimens but caused relatively minor reductions in peak residual lateral strength.

For example, SMF specimens experienced a 30% reduction in initial lateral stiffness (from 20 kN to 14 kN), while IMF specimens showed a 20% reduction (from 18 kN to 15 kN) at 1 mm displacement.

3. Displacement Behavior

Fire exposure increased the failure displacement of all specimens by approximately 25%, likely due to degradation of the bond between anchor and concrete caused by differential thermal expansion.

4. Residual Strength After Fire

A slight gain in residual strength was observed in some specimens after fire exposure. This is attributed to the thermal insulating properties of concrete, which limited internal temperatures to below 500 °C—temperatures at which concrete can experience strength gain.

5. Impact on Anchor Interfaces

Despite modest strength gains, degradation at the steel–concrete anchor interface may have occurred due to thermal effects, contributing to increased lateral displacements after fire.

6. Effectiveness of CFRP Strengthening

CFRP wrapping significantly enhanced both lateral strength and ductility of the specimens after fire.

CFRP also contributed to increased ductility, particularly in IMF specimens:

Post-fire ductility increased by 33% for SMF and 100% for IMF.

7. Consistency of CFRP Effects

CFRP wrapping showed a consistent positive effect on residual initial lateral stiffness across both SMF and IMF specimens, confirming its reliability as a post-fire strengthening method.

8. Model Accuracy:

The developed model successfully captures the experimental response of the specimens, accurately predicting behavior up to and beyond failure.

While this study provides an exploratory experimental program, more studies are required to elaborate on how the level of detailing of the reinforcement affects both residual capacity, stiffness of the steel–concrete anchorage zones, quantify crack widths, and correlate damage to load–displacement hysteresis.

Author Contributions: Conceptualization, A.A. (Amer Alkloub); methodology, A.A. (Amer Alkloub) and M.D.; software, M.D.; validation, A.A. (Amer Alkloub) and M.D.; formal analysis, A.A. (Amer Alkloub) and M.D.; investigation, A.A. (Amer Alkloub), M.D., A.A. (Ahmed Ashteyat) and F.S.; resources, A.J. and F.S.; data curation, A.A. (Ahmed Ashteyat); writing—original draft preparation, A.A. (Amer Alkloub) and M.D.; writing—review and editing, A.A. (Amer Alkloub) and M.D.; visualization, M.D., A.A. (Ahmed Ashteyat) and F.S.; supervision, A.A. (Amer Alkloub); project administration, A.A. (Amer Alkloub) and A.J.; funding acquisition, A.A. (Amer Alkloub) All authors have read and agreed to the published version of the manuscript.

Funding: Deanship of Scientific Research/the University of Jordan, Amman, Jordan, grant No. 2390.

Data Availability Statement: Data is contained within the article.

Acknowledgments: Amer Alkloub expresses his gratitude to the University of Jordan, Amman, Jordan, for supporting his sabbatical leave, during which this article is published.

Conflicts of Interest: The authors declare no conflict of interest.

References

1. *AISC 341-16*; Seismic Provisions for Structural Steel Buildings. American Institute of Steel Construction: Chicago, IL, USA, 2016.
2. *FEMA 350*; Recommended Seismic Design Criteria for New Steel Moment-Frame Buildings. Federal Emergency Management Agency: Washington, DC, USA, 2000.
3. Sabelli, R.; Roeder, C.; Hajjar, J.F. *Seismic Design of Steel Special Moment Frames: A Guide for Practicing Engineers*; NEHRP/FEMA/ATC-72; National Institute of Standards and Technology: Gaithersburg, MD, USA, 2003.
4. Baggio, D.; Soudki, K.; Noël, M. Strengthening of concrete structures with externally bonded fiber reinforced polymers in presence of elevated temperatures: A review. *Constr. Build. Mater.* **2014**, *63*, 65–80.
5. Kodur, V.K.R.; Ahmed, A. Fire resistance of CFRP-strengthened reinforced concrete beams. *Fire Saf. J.* **2010**, *45*, 21–29. [CrossRef]
6. ACI Committee. *ACI PRC-440.2-17: Guide for the Design and Construction of Externally Bonded FRP Systems for Strengthening Concrete Structures (ACI 440.2R-17)*; American Concrete Institute: Farmington Hills, MI, USA, 2017.
7. Covi, P.; Tondini, N.; Tornaghi, M.L.; Molina, F.J.; Pegon, P.; Tsionis, G. Seismic experimental analysis of a full-scale steel building with passive fire protections. *Eng. Struct.* **2024**, *300*, 117203. [CrossRef]
8. Verma, M.; Prakash, A.; Anandavalli, N. Investigations on the flexural performance of integrated laced steel-concrete composites (i-LSCC) panels. *Int. J. Prot. Struct.* **2024**, 20414196251328382. [CrossRef]
9. Li, S.; Liew, J.R.; Xiong, M.X. Fire performance of composite columns made of high strength steel and concrete. *J. Constr. Steel Res.* **2021**, *181*, 106640. [CrossRef]
10. Han, L.H.; Zhou, K.; Tan, Q.H.; Song, T.Y. Performance of steel reinforced concrete columns after exposure to fire: Numerical analysis and application. *Eng. Struct.* **2020**, *211*, 110421. [CrossRef]
11. Tian, K.; Ožbolt, J.; Sharma, A.; Hofmann, J. Experimental study on concrete edge failure of single headed stud anchors after fire exposure. *Fire Saf. J.* **2018**, *96*, 176–188. [CrossRef]
12. *ISO 834-11:2014*; Fire Resistance Tests—Elements of Building Construction—Part 11: Specific Requirements for the Assessment of Fire Protection to Structural Steel Elements. ISO: Geneva, Switzerland, 2014.
13. Hertz, K.D. Limits of spalling of fire-exposed concrete. *Fire Saf. J.* **2003**, *38*, 103–116. [CrossRef]
14. American Concrete Institute. *Building Code Requirements for Structural Concrete (ACI 318-25) and Commentary*; American Concrete Institute: Farmington Hills, MI, USA, 2025.

15. *ANSI/AISC 360-22*; Specification for Structural Steel Buildings. American Institute of Steel Construction: Chicago, IL, USA, 2022.
16. ANSYS, Inc. *ANSYS Multiphysics*; Version 2023 R1; ANSYS, Inc.: Canonsburg, PA, USA, 2024.
17. Xu, Y.; Shen, W.D.; Wang, H. An experimental study of bond-anchorage properties of bars in concrete. *J. Build. Struct.* **1994**, *15*, 26–37.
18. Kodur, V.K.R.; Dwaikat, M.M.S.; Dwaikat, M.B. High-temperature properties of concrete for fire resistance modeling of structures. *ACI Mater. J.* **2008**, *105*, 517–527.
19. Alfano, G.; Crisfield, M.A. Finite element interface models for the delamination anaylsis of laminated composites: Mechanical and computational issues. *Int. J. Numer. Methods Eng.* **2001**, *50*, 1701–1736. [CrossRef]
20. Alfano, G. On the influence of the shape of the interface law on the application of cohesive-zone models. *Compos. Sci. Technol.* **2006**, *66*, 723–730. [CrossRef]
21. Travush, V.I.; Kashevarova, G.G.; Martirosyan, A.S.; Avhacheva, I.A. Experimental study of possible ways to increase cohesion strength in the "steel-concrete" contact zone under displacement conditions. *Procedia Eng.* **2016**, *153*, 766–772. [CrossRef]
22. Pallares, L.; Hajjar, J. Headed steel stud anchors in composite structures, Part II: Tension and interaction. *J. Constr. Steel Res.* **2010**, *66*, 213–228. [CrossRef]
23. Qian, S.; Li, V.C. Headed Anchor/Engineered Cementitious Composite Pull Out Behavior. *J. Adv. Concr. Technol.* **2011**, *9*, 339–351. [CrossRef]
24. Robins, P.J.; Standish, I.G. The influence of lateral pressure upon anchorage bond. *Mag. Concr. Res.* **1984**, *36*, 195–202. [CrossRef]
25. Guezouli, S.; Lachal, A. Numerical analysis of frictional contact effects in push-out tests. *Eng. Struct.* **2012**, *40*, 39–50. [CrossRef]
26. Okada, J.; Yoda, T.; Lebet, J. A study of the grouped arrangements of stud connectors on shear strength behavior. *Struct. Eng. Earthq. Eng.* **2006**, *23*, 75s–89s. [CrossRef]
27. Nguyen, H.T.; Kim, S.E. Finite element modeling of push-out tests for large stud shear connectors. *J. Constr. Steel Res.* **2009**, *65*, 1909–1920. [CrossRef]
28. Lee, P.-G.; Shim, C.-S.; Chang, S.-P. Static and fatigue behavior of large stud shear connectors for steel–concrete composite bridges. *J. Constr. Steel Res.* **2005**, *61*, 1270–1285. [CrossRef]
29. Lin, J.P.; Wang, J.F.; Xu, R.Q. Cohesive Zone Model Based Numerical Analysis of Steel-Concrete Composite Structure Push-Out Tests. *Math. Probl. Eng.* **2014**, *2014*, 175483. [CrossRef]
30. Lim, O.K.; Choi, S.; Kang, S.; Kwon, M.; Choi, Y.J. Experimental Studies on the Behaviour of Headed Shear Studs for Composite Beams in Fire. *Steel Compos. Struct.* **2019**, *32*, 743–752. [CrossRef]
31. Lim, O.K.; Choi, S.; Kang, S.; Kwon, M.; Choi, J.Y. Fire performance of headed shear studs in profiled steel sheeting. *J. Constr. Steel Res.* **2020**, *164*, 105791. [CrossRef]
32. Purkiss, J.A. *Fire Safety Engineering Design of Structures*, 2nd ed.; CRC Press: Boca Raton, FL, USA; Butterworth-Heinemann: Oxford, UK; Linacre House: Birmingham, UK; Jordan Hill: Blyth, UK, 2007.